Structure Properties of Dextran. 2. Dilute Solution†

Catalina E. Ioan,‡,§ Thomas Aberle,‡ and Walther Burchard*,‡

Institute of Macromolecular Chemistry, University of Freiburg, 79104 Freiburg, Germany; and "P.Poni" Institute of Macromolecular Chemistry, 6600 Iasi, Romania

Received February 11, 2000; Revised Manuscript Received May 16, 2000

ABSTRACT: Dilute solution properties of 13 dextrans with different molar masses in water and 0.5 M NaOH were investigated. Seven of these samples were products of Sigma prepared by bacteria from *Leuconostoc mesenteroides*, one was obtained by fractionation of the dextran with the highest molar mass, and five samples were obtained by degradation via controlled acid hydrolysis. Static and dynamic light scattering, viscometry and analysis of the reducing end group were applied. The molar mass dependencies of the radius of gyration R_g, the hydrodynamic radius R_h, the second virial coefficient A_2 and the intrinsic viscosity $[\eta]$ for the nonfractionated samples were determined. The results are compared with data from the literature. Size exclusion chromatography in on-line combination with multiple-angle laser light scattering and viscosity detection revealed different calibration curves M_i vs V_e for the studied samples. The molar mass dependencies of the radii and intrinsic viscosities could be measured. The data of the radii of gyration from four fractionated samples were found to form one common curve. The intrinsic viscosities, on the other hand, gave two curves, one for the Sigma sample and another one for the acid-degraded samples. These findings are discussed in comparison with the nonfractionated samples. The polydispersity of dextrans, like those for other hyperbranched polysaccharides, increased strongly with M_w but weaker than predicted by theory. Generalized ratios $\rho = R_g/R_h$ and $V_r = A_2M_w[\eta]$ are considered and discussed in comparison with data from other laboratories and compared with predicted values. The coil−coil interpenetration function Ψ and the solvent-coil draining function Φ were found to increase with the molar mass as a result of increasing branching density.

Introduction

Bacterial polysaccharides have aroused interest for many years.[1,2] Among these dextran is probably the oldest one that has found much application.[3] Dextran is a branched polysaccharide (Scheme 1), composed of α-D-glucopyronosyl residues, all having preponderant the α(1→6) linkage. Some dextrans are composed almost exclusively of (1→6) linkage, whereas others may contain less than 50% of it. The other types of linkages may be (1→2), (1→3) or (1→4), so that a series of α-D-linked D-glucans containing a variety of linkage types is available.[1,4] There are different strains which synthesize products from glucose after cleaving sucrose of very different extent of branching. Commercially mostly used is a dextran from *Leuconostoc mesenteroides*, strain B-512(F), with an overall degree of branching of about 5%.[4] A large number of these branches appeared to be short, but the physical chemical properties are mainly determined by long chain branching which could be considerably smaller than 5%. However, also strains with branching density up to 30% were reported.[5] In contrast to other branched polysaccharides such as amylopectin and glycogen the branched topology is not well-known. In principle, however, also dextran, together with amylopectin and glycogen, belongs to the class of hyperbranched polymers, i.e., one has one focal end group (the reducing end group) and four other have nonreducing end groups per repeating unit.[6] This means the dextran can contain units where only two functionalities are used forming a linear chain, and it can contain trifunctional and tetrafunctional branching units.

Scheme 1. R_1, R_2, R_3: Short or Long Range Branching in C3 and C4-Position; In Total 4% Branching

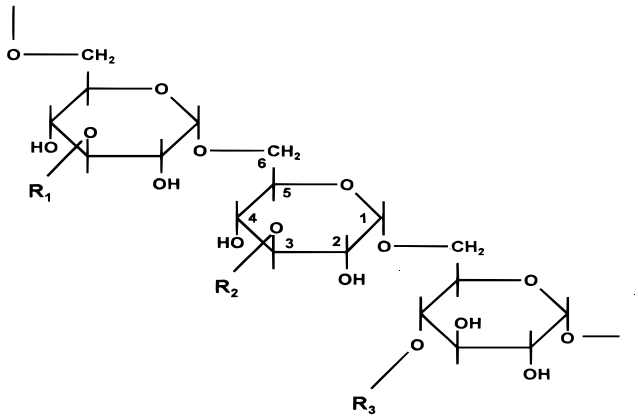

The solution properties of dextran have been repeatedly investigated.[7] A rather comprehensive paper was recently published by Nordmeier.[8] Despite the care he invested, several points remained still not fully clarified. For instance, the polydispersity was not taken into account, and also the size distribution and viscosity behavior were not considered. The present study was motivated by our interest in the semidilute solution behavior of branched polysaccharides, e.g., amylopectin, glycogen, and now dextran.[9] The study of the semidilute dextran solution has already been published. It is now appropriate to supply details of our results obtained in the dilute solution.

In the following we first will discuss (i) the properties of nonfractionated commercial available samples, and

† Dedicated to Professor Cristofor I. Simionescu,"P. Poni" Instiute of Macromolecular Chemistry, Iasi, Romania, on the occasion of his 80th birthday.

‡ University of Freiburg.

§ "P.Poni" Institute of Macromolecular Chemistry.

10.1021/ma000282n CCC: $19.00
Published on Web 07/07/2000

Table 1. Characteristic Parameters of Dextran Samples: D1−D7, SIGMA Dextrans; Df1, Fractionated D1; Dd1−Dd5, Acid-Degraded Samples

		SLS(λ_0 = 632.8 nm) in Water					SLS (λ_0 = 488 nm) in 0.5M NaOH					
sample	DS (%)	$10^{-4}M_w$ (g/mol)	10^5A_2 (mol·mL/g^2)	R_g (nm)	R_h (nm)	[η] (mL/g)	$10^{-4}M_w$ (g/mol)	10^5A_2 (mol mL/g^2)	R_g (nm)	R_h (nm)	[η] (mL/g)	$10^{-4}M_n$[a] (g/mol)
D1	92	266	5.4	47	47	61.0	270	7.1	50	46	81.1	8.43
D2	91	50.6	17.6	21	17	53.1	48.8	24.3	23	21	64.5	17.0
D3	94	33.4	20.2	19	15	46.1	35.6	28.9	21	19	57.2	3.94
D4	94	13.2	32.8	12	11	35.0	16.6	34.9	14	13	46.4	4.87
D5	89	5.90	45.6	-	10	26.3	6.84	40.8	-	8	30.4	4.20
D6	85	3.74	42.2	-	5	20.9	4.65	51.0	-	6	20.8	2.09
D7	92	0.90	74.9	-	3	8.6	1.18	59.9	-	4	9.3	0.48
Df1	92	290	5.0	45	38	67.8	301	6.2	52	48	76.7	18.2
Dd1	88	127	9.3	33	29	62.1	173	11.3	39	35	60.5	19.2
Dd2	85	52.2	15.1	29	26	49.8	64.3	15.5	30	27	48.8	12.2
Dd3	87	16.1	21.9	14	11	28.9	16.1	38.5	18	16	32.1	3.71
Dd4	84	7.75	38.0	-	9	18.1	9.35	58.6	-	10	19.3	1.59
Dd5	87	6.62	37.6	-	9	16.4	7.77	32.3	-	10	18.5	2.24

[a] End group analysis; method of Nelson-Somogyi.

(ii) of some polydisperse fractions which were prepared by degradation from the high molar mass dextran D1. Static and dynamic light scattering and viscometry were applied, and the number-average degree of polymerization was determined by spectroscopic end group determination. The second part deals with size exclusion chromatography (SEC) in on-line combination with multi angle laser light scattering (MALLS) and viscometry (VISC). These measurements gave results on the size distribution and on the molar mass dependence of the radius of gyration and the intrinsic viscosity. Similar studies were made previously by a few other authors. Kulicke et al.[10] applied the cross-flow field flow fractionation. He focused his attention mainly to a check of the separation possibilities of this new technique. Hanselmann et al.[11] had no MALLS detector available and determined the distribution with the aid of low angle laser light scattering (LALLS) and VISC detectors. In contrast to these earlier measurements the present paper makes use of the full power of this combination method. From these data shrinking factors g (=$R_{g,b}/R_{g,lin}$) and g' (=$[\eta]_b/[\eta]_{lin}$) could be determined if data from the linear reference system were available. Although such reference does not exist, these factors could still be estimated under certain assumptions. The problem is involved and will be discussed at some length in a separate paper. Furthermore, the coil−coil interpenetration function Ψ will be derived from the second virial coefficient and the draining function Φ in the Fox−Flory equation from the intrinsic viscosity. Both functions give interesting insight into the local segment density distribution of the macromolecules.

Experimental Section

Samples. Seven dextrans, products of Sigma (D1−D7), prepared by bacteria from *L. mesenteroides*, with different molecular weights were analyzed with regard to M_w, M_n, A_2, R_g, R_h, and [η] (see Table 1). To obtain fractions of different molar masses, a controlled degradation by acid hydrolysis was carried out.[12] The high molar mass dextran (D1) was suspended in methanol and different amounts of concentrated HCl were added at room temperature (1 g of glycogen + 4 mL of MeOH + x mL of HCl, with x = 0.04, 0.12, 0.20, 0.28, and 0.36, respectively). Each mixture was shaken for 4 days when, according to literature,[12] the limiting value is reached. The degraded samples Dd1−Dd5 were neutralized with 1 M NaOH and washed with methanol. Also, a fractionation of D1 was made to obtain a sample Df1 with a narrower distribution. Therefore, methanol was added to the aqueous solution and the precipitated parts isolated. Measurements were carried out at 20 °C. Water with 0.01% sodium azide (NaN_3) added and 0.5 M NaOH were used as solvents.

Dry substance content was determined in a moisture analyzer (Sartorius MA 40). The obtained values were between 84 and 94%.

Number-Average Molecular Mass. M_n was obtained by the reducing end group determination, following the method of Nelson−Somogyi.[13]

Static Light Scattering (SLS). Measurements were performed with two fully computerized and modified SOFICA photogoniometers (G. Baur, Instrumentenbau, Hausen, Germany). The one was equipped with a He−Ne laser (λ_0 = 632.8 nm) and the other with an Ar-ion laser (λ_0 = 488 nm). Measurements were made in an angular region from 35 to 145°, in steps of 5°, at 20 °C. Two different solvents were used, i.e., water and 0.5 M NaOH, with the refractive index increments dn/dc = 0.151 mL/g (for water and λ_0 = 632.8 nm) and dn/dc = 0.142 mL/g (for NaOH and λ_0 = 488 nm).[14]

Dynamic Light Scattering (DLS). Measurements were carried out using an ALV photogoniometer (ALV, Langen, Germany) equipped with an ALV 5000 correlator. Measurements were made in an angular range from 30 to 150°, in steps of 10°, at 20 °C. For details see ref 15.

Size Exclusion Chromatography (SEC). Analytical fractionation of the samples was carried out by SEC in on-line combination with an multiangle laser light-scattering (MALLS) instrument (DAWN, Wyatt Technology, Santa Barbara, CA) and with a RI/VISC detector (Knauer, Berlin, Germany), that allowed the detection of concentration and viscosity. The chromatography was driven by an HPLC pump 64 (Knauer, Berlin, Germany) at a pressure of 10 bar. The injection volume was 50 μL. As elution solvent a 0.1 M $NaNO_3$ solution containing 0.05% NaN_3 was chosen. The addition of sodium azide was necessary to prevent bacterial growth. For the degraded samples a two-column system, 2xPL aquagel-OH Mixed 8 μm, from Polymer Laboratories Heerlen, NL was used. For the Sigma dextrans an additional PSS Suprema 10000, 10 μm column, from Polymer Standards Service (Mainz, Germany)) was employed. For the high molar masses (D1, D2 and Df1) also a four-column system was used, i.e., a PSS Suprema 30000, 20 μm column, from Polymer Standards Service (Mainz, Germany) in addition to the mentioned three.

Viscosity. Measurements were made with an automatic Ubbelohde viscometer (Schott, Germany) at 20 °C in water and in 0.5 M NaOH. A capillary of 0.63 mm in diameter was used.

Results

Properties of Nonfractionated Samples. Measurements were performed in two solvents, i.e., water and 0.5 M NaOH, by static and dynamic light scattering and viscometry. The data of M_w, A_2, R_g, R_h, [η], and M_n are collected in Table 1. The radii of gyration R_g and

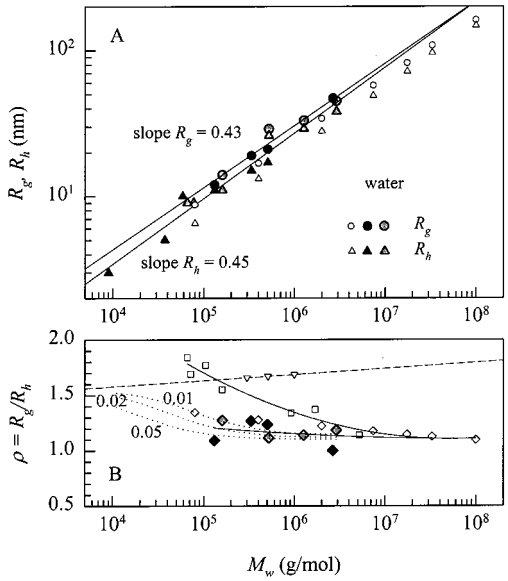

Figure 1. (A) Molar mass dependencies of the radius of gyration (circular symbols) and the hydrodynamic radius (triangular symbols) for different samples in water: (▲), (●) dextrans−Sigma; (gray triangle), (gray circle) dextrans-degraded; (△), (○) dextrans−Nordmeier.[8] (B) The ratio $\rho = R_g/R_h$ of the two radii as a function of the molar mass M_w: (◆) dextrans−Sigma; (gray tilted square) dextrans-degraded; (◊) dextrans−Nordmeier;[8] (▽) pullulan−Nordmeier[8] (dashed line: fit); (□) degraded starches;[9a] doted lines, calculated with eq 4 for branching probabilities $p(1-p) = 0.01$, 0.02, and 0.05.

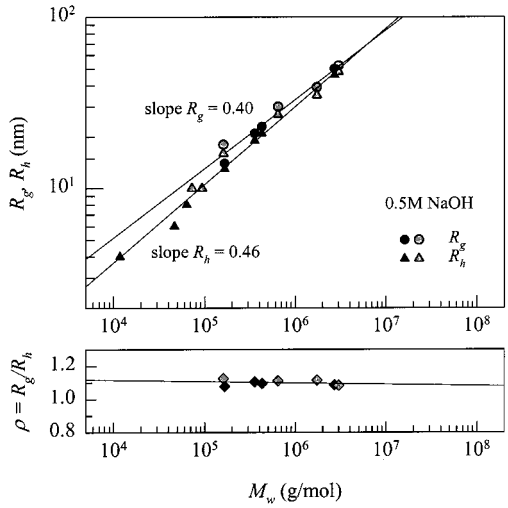

Figure 2. Molar mass dependencies of the radius of gyration (circular symbols) and the hydrodynamic radius (triangular symbols) for different samples in 0.5 M NaOH: The symbols are the same as in Figure 1. The lower part shows the ρ parameter (line: regression through the points).

the hydrodynamic radii R_h are plotted against the molar mass M_w in Figure 1 for water and in Figure 2 for 0.5 M NaOH. Underneath these figures the ratio of $R_g/R_h \equiv \rho$ is plotted, again against the molar mass M_w. For comparison also the data obtained by Nordmeier[8] are shown. In all cases the slope for the radius of gyration is smaller than for the hydrodynamic one. In all measurements, the ρ-parameter approaches at large M_w a constant value of $\rho = 1.09$. This is lower by a factor of 1.12 than predicted by the theory for hyperbranched polymers.[16] This asymptotic value is independent of the branching density. The effect of branching becomes noticeable at molar masses lower than 10^5 g/mol. The dotted lines correspond to theoretical calculations to be

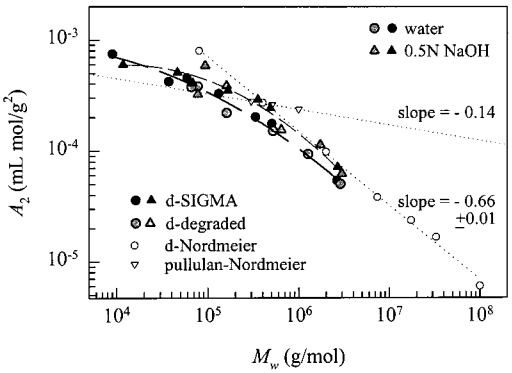

Figure 3. Molar mass dependency of the second virial coefficient A_2 for the studied dextrans samples in water and 0.5 M NaOH. For comparison, literature data[8] for dextran and pullulan in water are also presented. For details, see text. Note the difference in asymptotic slope between linear and branched samples.

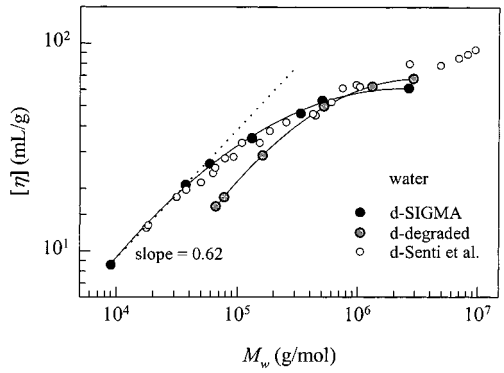

Figure 4. Molar mass dependency of the intrinsic viscosity $[\eta]$ for dextran in water. The data by Senti et al. were taken from the literature.[7] The dotted line corresponds to the initial slope at low M_w, where no branching is expected.

discussed later in this paper. No difference was observed between the commercial samples and the series of acid-degraded dextrans. The molar masses determined by Nordmeier[8] are systematically about 10% larger than our values. Very likely this is a result of calibration error of his or our instruments. On the whole the agreement is good.

Figure 3 shows the molar mass dependence of the second virial coefficient A_2. Again the data by Nordmeier are shifted to higher molar masses by the same factor as found for the radii. In particular the asymptotic slope is the same, also for both solvents, and has a value of -0.66 ± 0.01. This slope is appreciable more negative than the value that was found for pullulan.[8] The virial coefficients in NaOH are in general slightly larger than in water and indicate NaOH as the better solvent. Interestingly, at low molar masses the data come together. Only the value for the lowest molar mass from Nordmeier is considerably larger. However, we think, the experimental error in this region might be much larger than indicated by Nordmeier,[8] who apparently tried to fit his data by a simple power law. The observed deviation from the power law is a clear indication that asymptotic behavior is not yet reached in this low molar mass region.

Figures 4 and 5 show the intrinsic viscosity as a function of molar mass in water and 0.5 M NaOH, respectively. Surprisingly, the two series of the commercially available and of the degraded samples now differ from each other. In Figure 4 also data obtained

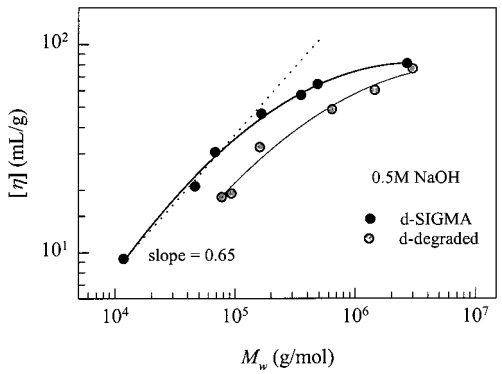

Figure 5. Molar mass dependency of the intrinsic viscosity [η] for dextran in 0.5 M NaOH. Description as in Figure 4.

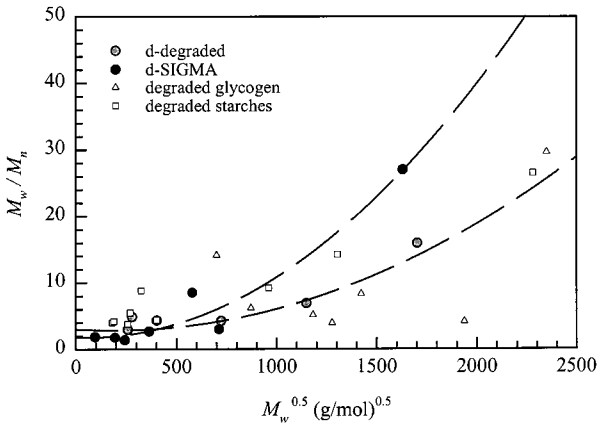

Figure 6. Polydispersity of dextran as a function of the root of the molar mass M_w for dextran in comparison with degraded glycogen[9c] and degraded starches.[12] This comparison appeared of interest, because degradation may have caused partial debranching. The dashed lines represent regressions to Sigma dextrans and the degraded ones. M_n was determined by end group analysis and M_w by static light scattering. See also Table 1 and comment on M_n in the text.

by Senti et al.[7] are plotted and show good agreement. Power law behavior seems to be approached only in the small molar mass region. The reason for a nonlinear Kuhn-Mark−Houwink relationship will be discussed later.

Polydispersity. In contrast to linear chains the polydispersity ratio M_w/M_n remains not constant for different weight-average molar masses. According to branching theory this ratio starts at a value of 2 and increases then drastically.[6,17] For randomly branched materials the ratio increases with M_w and becomes infinitely large at the gel point.[6] For hyperbranched structures the polydispersity ratio increases asymptotically only with $M_w^{0.5}$.[17] A gel point is never reached. In view of this theoretical predictions it was of interest, to know how the polydispersity of the dextrans varies with the molar mass. A check was possible because the reducing end group could be determined by a color reaction and ensuing spectroscopy. The reaction with the end group consists mainly of Cu^{2+} reduction to Cu^{+}. The sensitivity of this reaction was enhanced by a procedure of Nelson−Somogyi[13] and turned out to be very sensitive such that number averages up to $M_n \cong$ 200 000 g/mol could be detected, corresponding to a DP_n of about 1000.

Figure 6 shows the results of the polydispersity ratio for dextran, degraded starches,[12] and degraded glycogens.[9c] The weight-average molar mass M_w was determined by static light scattering and the number-average molar mass M_n by end group determination. The M_n data from SEC were here not considered because of the well-known systematic errors. Despite the fairly large scatter of data the values from the different polysaccharides follow approximately one common line. The polydispersity increases first slowly, because in this range the macromolecule first consists of linear chains and later contains only a few branches. The asymptotic region with its strong increase in polydispersity is apparently attained when the molar mass M_w is larger than 2×10^6 g/mol. The upper curve in Figure 6 corresponds to a fit through the data of the commercial samples. The fairly strong difference could be real, but if the point with the largest polydispersity is neglected, no significant difference would be detectable. Interestingly the plot of M_n vs M_w approaches a power law behavior with an exponent of 0.499 ± 0.2, as theoretically expected, but at low M_w the M_n decreases stronger. This again is in agreement with the Cascade theory[17] for hyperbranched samples. The experimental error is certainly lower than 10% and this leads to the conclusion that the scatter of data is related to inherent quantities of the samples. There may be a variation in the branching type, i.e., short chain and long chain branching.

The large polydispersity ratio of these branched materials will have a strong influence on the measured structural properties.[9] To elucidate this effect we turned to the determination of the molar mass distribution and the radii and the viscosity of the individual fractions.

Properties of Fractionated Samples. Recently, the common size exclusion chromatography (SEC) has been further developed by the on-line detection of concentration via a refractometer, multiangle laser light scattering (MALLS) and viscosity (VISC). Under ideal conditions such a setup should admit determination of the molar mass distribution and the radii of gyration and intrinsic viscosity as a function of molar mass. Unfortunately, no ideal separation into monodisperse fractions can be achieved by the SEC columns available on the market. Furthermore, accurate measurements of the molar mass, the radii of gyration and intrinsic viscosities are possible if the corresponding signals are large enough. These conditions are realized only in a certain region around the mean of the distribution. The mentioned problems may be demonstrated with dextran D1. If simply the soft ware of the DAWN instrument is used, one obtains a calibration curve as shown in Figure 7a. A simple straight line was expected but this is realized only in the restricted molar mass region from 2×10^5 to 5×10^6 g/mol. The deviation at large elution volume results probably from an incomplete separation. A very small fraction of large molecules is dragged through the column into the region where most of the samples have a much lower molar mass. Unfortunately, in light scattering even very small numbers of large particles dominate the scattering behavior. Thus, much larger molar masses are found than for the majority of the macromolecules at that elution volume. On the other hand, a calibration with well fractionated samples showed that even in this large elution volume region a linear decrease of the molar mass with elution is obtained. We tried to increase the separation by using 2 columns (2xPL aquagel-OH Mixed 8 μm), 3 columns (the two column system plus a PSS Suprema 10000, 10 μm column) and 4 columns (the three column system

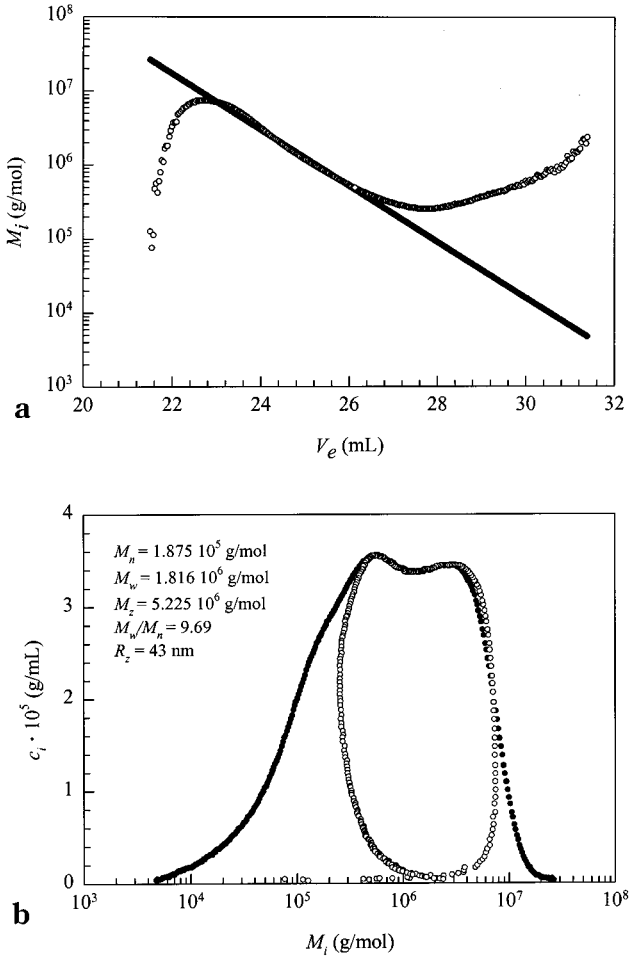

Figure 7. (a) Dependence of the molar mass on the elution volume in SEC−MALLS for D1 (open circles). Large scatter occurs at the edges of high and low molar masses. The filled symbols correspond to linear extension into these regions. (b) Molar mass distribution derived from SEC−MALLS (open symbols) and the calibration curve shown in Figure 7a (filled circles). The unusual behavior makes no sense and is the result of bad separation. On the contrary the filled symbols represent a reasonable molar mass distribution.

plus a PSS Suprema 30000, 20 μm column). The separation remained not satisfactory. Still an effect of improved separation can be seen in Figure 7b where the molar mass distribution was calculated from the measured raw data. Clearly, the bimodal structure becomes better modeled when passing from the two-column to the four-column setup (Figure 8). On the whole, however, senseless distributions are obtained with the raw data if only two columns are used; but it becomes increasingly better with the overall length of the columns. The data obtained with the different columns are listed in Table 2 and may be compared with these in Table 1.

In another approach we extended the linear section of the elution volume to both ends and recalculated with this modified calibration curve the molar masses. The justification of such procedure was checked previously in our laboratory with branched polystyrene and dextran derivatives.[11,18] A considerable improvement of the distribution was now found. In particular, when using the four-column system, nearly the same weight-average of the molar mass M_w was obtained, as found by static light scattering. Still the number-average molar mass M_n was found much too large. The separation in the low molar mass region was apparently not sufficient. Altogether, we have determined the distributions from 7 commercial dextrans and from 5 samples prepared by degradation. One sample was obtained by fractionation, using D1. The low molecular weight tail was removed by precipitation of the aqueous solution with methanol. When using the modified calibration curves a very satisfactory agreement of the weight-average molar mass with the directly measured ones were obtained. However, the polydispersity was found in all cases being considerably narrower. Figure 9 shows for the two series of samples the modified calibration curves. The corresponding distributions are shown in Figure 10. The results now are looking reasonable.

Molar Mass Dependencies of the Radii and Intrinsic Viscosities. Figure 11 shows the result of the radius of gyration R_g as a function of the molar masses M_i for the various slices of the SEC. Because of the low dimensions only four samples were analyzed. These are D1, D2, D3, and D4. Only sections from reliable signals were used. Very satisfactory agreement is observed for the different samples with a strikingly low slope of 0.3. For comparison a dashed line is shown which corresponds to linear pullulan,[8] recalculated for most probable distribution (i.e., $R_g = R_{g,Nordmeier} \times 1.5^{1/2}$). This modification is required, because in the limit of no branching, i.e., low molar mass M_w, a polydisperse linear chain is obtained. The open triangle symbols correspond to the *z*-average of the nonfractionated samples. For the black triangles the radii were corrected for the weight-average according to

$$R_{g(w)} = R_{g(z)}\left(\frac{M_w}{M_z}\right)^{1/2} \quad (1)$$

The ratios of M_z/M_w and M_w/M_n are shown in Figure 12. For the evaluation of M_z, see the Discussion.

Figure 13 shows the corresponding results for the viscosity. The symbols are the same as shown in Figure 11. In addition the data by Senti et al.[7] are shown. A very satisfactory agreement between the nonfractionated and the fractionated samples was found. In particular the curvature is reproduced with the fractions. Only at very high molar masses do the curves spread. The straight line was drawn through the initial points of measurements. In this region we can expect linear chain behavior, because for the branching density for about 3−5% the number of branching points can be expected to be very small. The slope 0.62 corresponds to expectation for linear chains in a fairly good solvent.[19]

Discussion

The molar mass dependencies of the radius of gyration R_g, the second virial coefficient A_2 and the intrinsic viscosity $[\eta]$ follow for flexible linear chains power law behavior. These relationships are related to the fractal dimension $d_f = 1/\nu$. The various exponents are correlated via scaling laws which are for A_2 and $[\eta]$ as follows:

$$a_{A_2} = 3\nu - 2 = 3/d_f - 2 \quad (2)$$

$$a_{[\eta]} = 3\nu - 1 = 3/d_f - 1 \quad (3)$$

The exponents found for nonfractionated and fraction-

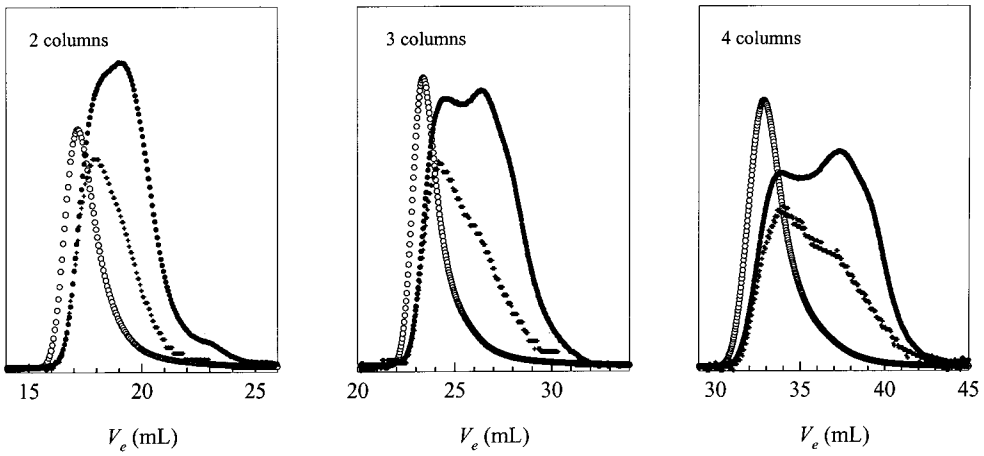

Figure 8. Improvement of separation when using two, three and four columns, respectively, demonstrated with sample D1: (○) LS; (●) RI; (+) VISC signals.

Table 2. Average Molecular Weights and *z*-Average Radius of Gyration Derived from SEC in On-Line Combination with MALLS (λ_0 = 632.8 nm) and VISC (for Details See Text; Compare also Table 1)

sample	$10^{-4}M_n$ (g/mol)	$10^{-4}M_w$ (g/mol)	$10^{-4}M_z$ (g/mol)	R_z (nm)
		4 Columns		
D1	26.5	278	829	44
D2	20.7	44.9	107	25
Df1	72.3	334	892	44
		3 Columns		
D1	18.8	182	523	43
D2	19.0	41.8	99.2	24
D3	6.84	27.8	98.6	22
D4	4.36	14.2	39.0	19
D5	3.99	6.53	10.0	11
D6	1.89	3.31	5.13	10
D7	0.58	0.83	1.11	-
		2 Columns		
Df1	128	332	586	49
Dd1	41.6	129	287	33
Dd2	15.3	58.3	15.6	30
Dd3	4.73	15.3	47.3	23
Dd4	1.68	4.30	9.55	20

ated samples are for the radii of gyration

$$\langle \nu \rangle = 0.43$$

$$\nu_f = 0.30$$

which would correspond to fractal dimensions of

$$\langle d_f \rangle_e = 2.33$$

$$d_f = 3.33$$

Here $\langle d_f \rangle_e$ denotes the ensemble average fractal dimension and d_f that for individual clusters. The $\langle d_f \rangle_e$ of the dextrans agrees almost exactly with that for starches.[20] The difference between the two values of the fractal dimensions is common for randomly branched materials[21] and is a result of an influence of polydispersity M_z/M_w. However, the observed cluster fractal dimension would be with 3.33 larger than for hard spheres which would be physically meaningless. However, the low exponent and the apparently too large fractal dimension could be caused by an increase of the branching density (number of branching points/per total number of repeating units), i.e., the branching density would increase with the size of the cluster. This conjecture is confirmed by the intrinsic viscosity which in contrast to scaling prediction shows no power law behavior. The flattening of the curves at high molar mass is in agreement with an increased branching density. The quantitative details will be discussed in the mentioned consecutive paper. The second virial coefficient A_2, on the other hand, asymptotically approaches power law behavior with an exponent of −0.66. Power law behavior was also found

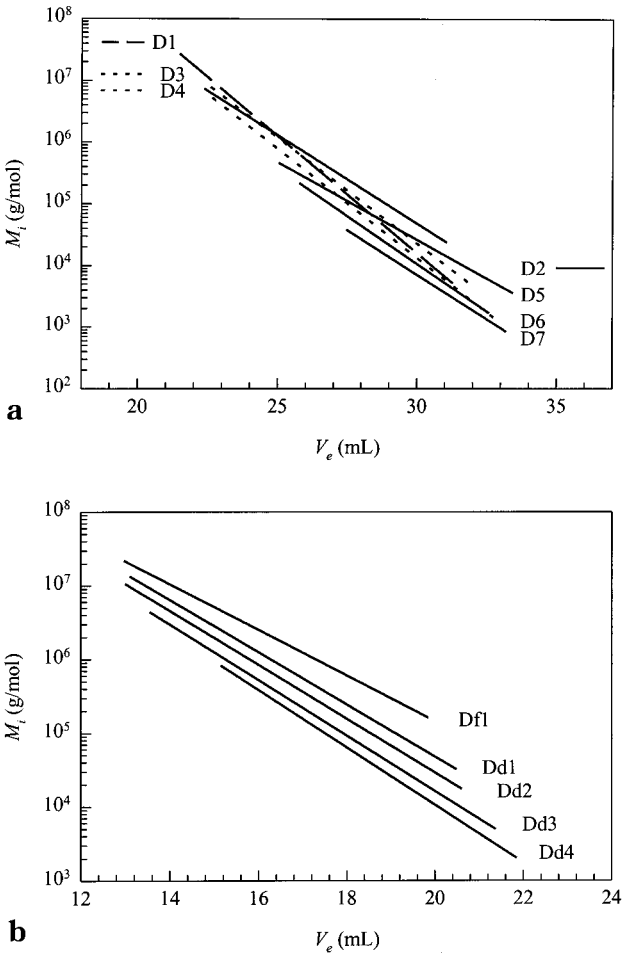

Figure 9. Calibration curves for (a) Sigma dextrans (D1−D7). The different slopes indicate different branching structures. Four samples (D2, D5−D7) seem to be of the same origin; (b) Calibration curves for degraded (Dd1−Dd4) and fractionated (Df1) dextrans, derived from D1. Degradation apparently causes a change in the branching structure.

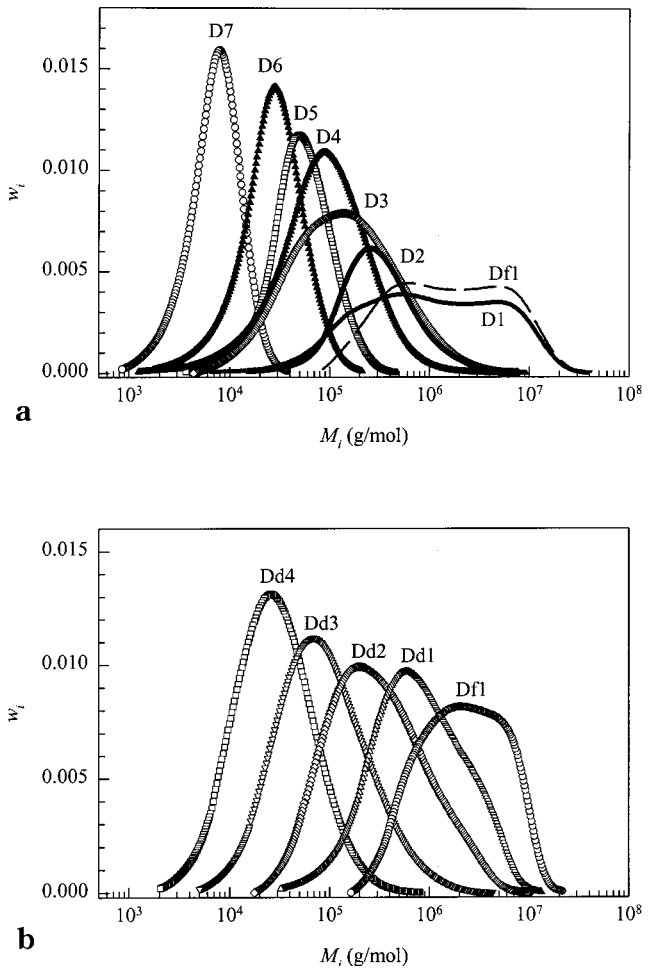

Figure 10. Distribution functions of (a) the Sigma samples and (b) the degraded ones. The curves of Figure 10a were obtained with a three-column set, with the exception of D1 and Df1, where four columns were used. The curves in Figure 10b were obtained with a two columns set. Note: The difference of separation power when comparing Df1 in parts a and b.

by Nordmeier.[8] Applying the scaling law of eq 2 this would give $\nu_{A_2} = 0.45$ and $d_{fA_2} = 2.24$, when the measured exponent $\langle\nu\rangle$ is used. The agreement is surprisingly good, the small deviation between $\langle\nu\rangle$ and ν_{A_2} may have a physical background. The somewhat weaker decrease of A_2 than predicted from the exponent $a_{A_2} = -0.71$ may be caused by an increase of the coil−coil interpenetration factor Ψ. This behavior is in fact observed.

Generalized Ratios. Recently generalized and dimensionless ratios have aroused much interest because it is hoped that these would give special information on the architecture of the macromolecules.[22] The one is the ρ parameter $\rho = R_g/R_h$ and the other is $V_r = A_2M_w/[\eta]$, which is the ratio of two volumes. The ρ parameter has been already shortly discussed. In addition to that we mention that this parameter decreases with the branching density. For hyperbranched structures an asymptotic value of $\rho = 1.225$ was theoretically predicted[16] on the basis of the Kirkwood−Riseman preaverage approximation[23] for hydrodynamic interaction. Later Freire and co-workers[24] showed by Monte Carlo and Brownian motion simulations that this Kirkwood approximation underestimates the effect of hydrodynamic interaction by about 13−24% which would reduce the predicted asymptotic limit to $\rho = 1.08-0.98$.

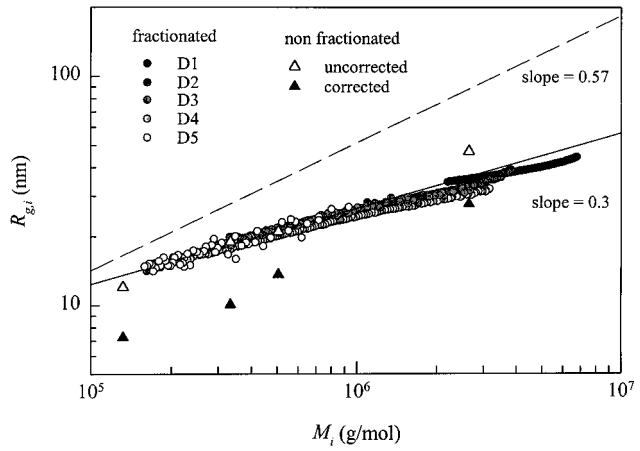

Figure 11. Molar mass dependence of the radius of gyration obtained with the five Sigma samples D1, D2, D3, D4, and D5, using the SEC−MALLS technique. The data form one common curve. The increase in the radii is unusually weak with a slope of 0.3, corresponding to an apparent fractal dimension of $d_{f,app} = 3.33$. However, the curve is not really described by a single power law. The initial slope is higher than the asymptotic one, indicating an increase of branching density with molar mass. The dashed line represents the molar mass dependence of pullulan in water,[8] corrected for most probable polydispersity. The open triangles represent the *z*-average of the radius of gyration of the nonfractionated samples, the filled triangles correspond to the weight averages, where the corrections were made from the data of Figure 12.

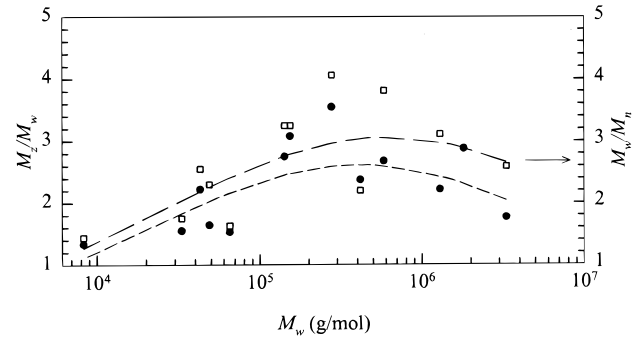

Figure 12. Polydispersity ratios M_z/M_w (●) and M_w/M_n (□) for all samples used. The data were obtained from SEC−MALLS. The dashed curves were drawn to guide the eye.

Experimentally, we found a value of $\rho = 1.09$. The effect of different branching densities becomes visible at smaller molar masses. The dotted lines in Figure 1 correspond to theoretical predictions. The corresponding equation[25,26] is

$$\rho = \left(\frac{3(1+2B_n)}{4(1+B_n)}\right)^{1/2}\left(\frac{2+B_n}{1+B_n}\right)0.89 \qquad (4)$$

$$B_n = p(1-p)DP_n$$

where the last factor corresponds to the correction for the baseline. B_n denotes the number of branching units in the macromolecules based on the number-average DP.

The scatter of the data are too large for distinguishing between branching densities of 1 and 5%. However, the tendency is more to the smaller branching densities. For comparison the data of the degraded starches are shown. Much stronger influence of the branching is

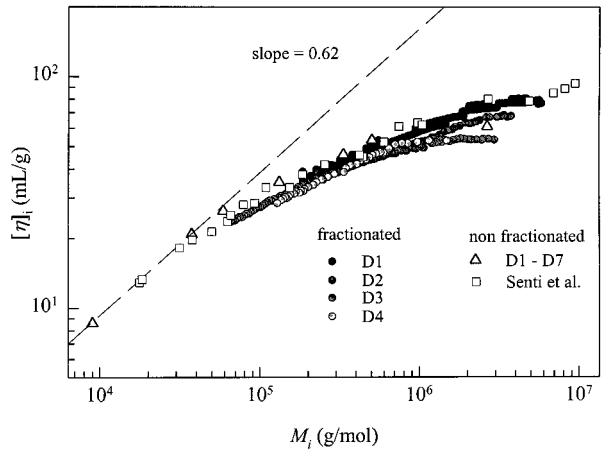

Figure 13. Intrinsic viscosity dependence on the molar mass for the same samples as shown in Figure 11 (excepting D5). The results were obtained from SEC−MALLS in combination with a viscometer VISC. The open squares are data from Senti et al.[7] and the open triangles corresponds to the nonfractionated samples. The dashed line represents the initial slope at small molar masses, that may be related to linear dextrans.

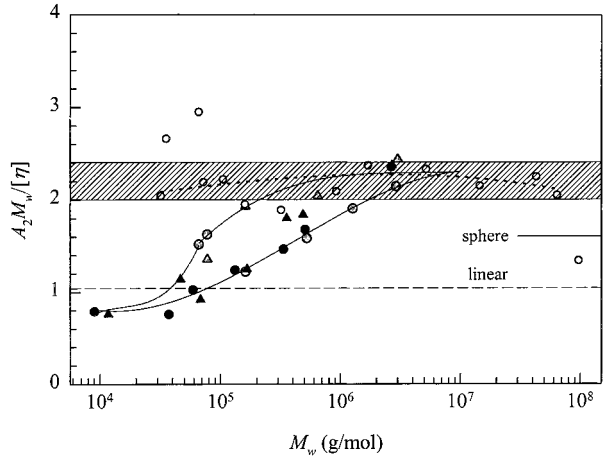

Figure 14. Molar mass dependence of the ratio $A_2M_w/[\eta]$. Black symbols are for Sigma dextrans in water (●) and in 0.5 M NaOH (▲). The shaded symbols refer to the degraded dextrans in water (gray circle) and in 0.5 M NaOH (gray triangle), respectively. The open circles are data from degraded starches.[9a] The shaded area represents the range of experimental error. The dashed line represents the values for linear chains.

noticeable. This behavior could be caused by favored cleavage of the branching points in the course of the special degradation technique applied to the samples.

The second generalized ratio V_r of the two volumes from A_2 and $[\eta]$ (see Figure 14) shows a more complex behavior. Again we have compared the data from dextran and starches. A constant value is theoretically expected in the limit of large molar masses for reasons that may be explained by the following equation:

$$V_r \equiv \frac{A_2 M_w}{[\eta]} = \frac{4\pi^{3/2} N_A (R_g^3/M)\Psi}{\Phi (R_g^3/M)} = 4\pi^{3/2} N_A \frac{\Psi}{\Phi} \quad (5)$$

In this equation Ψ is called the coil−coil interpenetration function and Φ the draining factor or the solvent-coil penetration function. For linear chains theory predicts[6,22] for both quantities asymptotically constant values of

$$\Psi^* = 0.269$$

$$\Phi^* = 3.96 \times 10^{24}$$

A value of $V_r = 1.04$ is predicted for linear chains. Our results show that a constant asymptote is reached but with twice the value as found for linear chains. Similar behavior was observed previously with randomly branched samples[27] and with the degraded starches,[9a] where the latter are also plotted in Figure 14.

Surprisingly the commercial available Sigma dextran values approach this limit more slowly than the data obtained by acid degradation. We are not able to give a simple explanation for this behavior because the hydrodynamic interaction as a function of branching density is yet not sufficiently well understood.

Effects of Polydispersity. With the data of R_g, A_2, and $[\eta]$, $\langle\Phi\rangle$ and $\langle\Psi\rangle$ can be calculated with the aid of the following two equations:

$$A_2 = 4\pi^{3/2} N_A \frac{(\langle R_g^2\rangle_z)^{3/2}}{M_w^2}\langle\Psi\rangle \quad (6)$$

$$[\eta] = \langle\Phi\rangle \frac{(\langle R_g^2\rangle_z)^{3/2}}{M_w} \quad (7)$$

Angle brackets are used to indicate that these parameters are those from polydisperse systems. Unfortunately, these quantities are derived from ratios of two different average types. Thus, the derived values became physically senseless when applied to systems with a broad size distribution. A simple correction can be made by transforming the z average of $\langle R_g^2\rangle_z$ into the weight-average.

$$\langle R_g^2\rangle_w \cong \left(\frac{M_w}{M_z}\right)^{3\nu} \langle R_g^2\rangle_z \quad (8a)$$

$$\langle R_g^2\rangle_n \cong \left(\frac{M_n}{M_z}\right)^{3\nu} \langle R_g^2\rangle_z \quad (8b)$$

The ratio of two weight averages is rather insensitive to a broad size distribution.

The correction for $\langle\Phi\rangle$ is more complex. As shown by Marriman and Herman[28] the intrinsic viscosity of polydisperse systems is given by

$$[\eta] = \Phi \frac{\langle R_g^3\rangle_n}{M_n} \cong \Phi \frac{(\langle R_g^2\rangle_n)^{3/2}}{M_n} \quad (9)$$

The finally corrected data are then given by eq 10

$$= \left(\frac{M_z}{M_w}\right)^{3\nu} \langle\Psi\rangle \quad (10)$$

$$\Phi = \left(\frac{M_z}{M_w}\right)^{3\nu} \left(\frac{M_w}{M_n}\right)^{3\nu - 1} \langle\Phi\rangle \quad (11)$$

The result of Φ and Ψ are shown in Figure 15, where also the data for degraded starches[9a] are plotted. With the exception of the highest molar mass of the dextrans the Φ parameter increased strongly with the molar mass, but remained smaller than the value of impenetrable spheres. The reason this highest molar mass

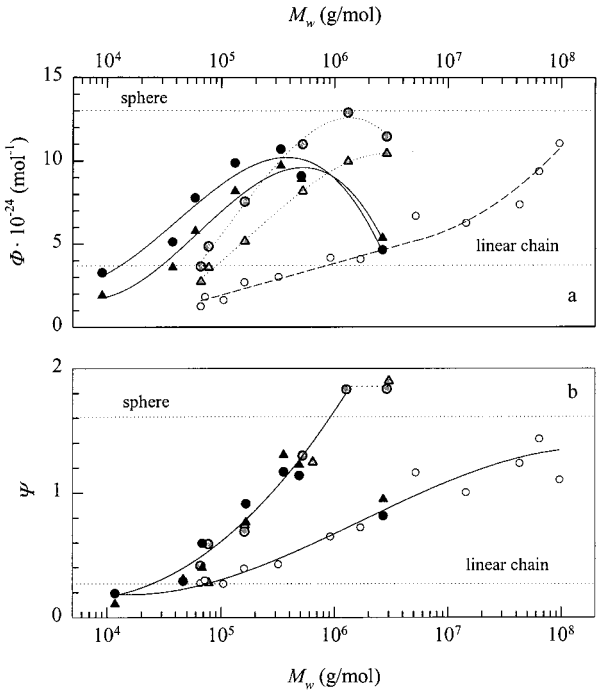

Figure 15. Molar mass dependence of (a) the draining function Φ and (b) of the coil−coil interpenetration function Ψ. The symbols are the same as in the previous Figures. The lines are drawn to guide the eye. For details see text.

deviates so strongly is not understood. A similar tendency is observed with the coil−coil interpenetration function, where the value for hard spheres is even exceeded, but still may be within the experimental error. The increase of both, the Φ and Ψ, can be considered as a result of an increased branching density with increasing molar mass. The initial part can be approximated with a power law for the exponents of $s = s_\Phi = s_\psi = 0.50$ (± 0.01) for the dextrans and $s = 0.31$ (± 0.02) for degraded starches. In earlier measurements from end-linked polystyrene stars an exponent of $s_\Phi = 0.28$ was found.[18] Thus, the slope is a measure of the branching efficiency.

The correction procedure depends much on the accuracy in the determination of the polydispersity. In SEC experiments the maximum of the light scattering elution curve is often taken proportional to the *z*-average of the molar mass.[29] We checked this conjecture and plotted M_{max} against the *z*-average M_z as determined from SEC (Figure 16a). The two quantities were found not only proportional to each other, but within the experimental error also the absolute values agree with each other. The measured data of M_z and M_n as a function of M_w are summarized in Figure 16b.

Conclusion

After studying the structure of amylopectins and glycogens with branching densities of ca. 4% and 8%, dextran was chosen as another branched polysaccharide, which like the others was suspected to show hyperbranched behavior. This conjecture was found to be correct. All three polysaccharide types could approximately be described by hyperbranching theory.

In contrast to linear chains power law behavior is observed only asymptotically at large M_w. In fact short chains do not contain branching points.

The effect of branching is best recognized from the molar mass dependencies of A_2 and $[\eta]$.

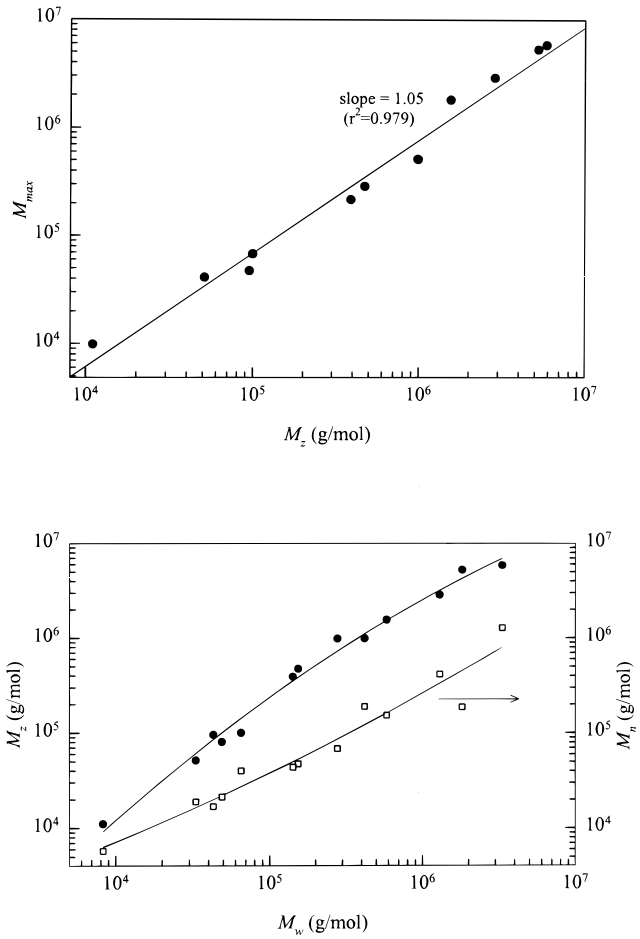

Figure 16. (a) Molar mass of the intensity maximum in SEC (M_{max}) as a function of the *z*-average molar mass M_z. Both quantities are not only proportional to each other, but coincide within experimental error also in value. (b) M_z and M_n as a function of M_w according to SEC measurements.

It also can be concluded from the exponent for R_g vs M_w of the SEC-fractions. Furthermore, the calibration curves of log M_i against V_e exhibit characteristic changes as the branching density varies.

Acknowledgment. We thank the Deutsche Forschungsgemeinschaft for loaning the SEC−MALLS instrument, which was given for studies of cellulose derivatives within the "Schwerpunkt: Cellulose and Cellulose Derivatives."

References and Notes

(1) Kenne, L.; Lindberg, B. Bacterial Polysaccharides. In *The Polysaccharides*; Aspinall, G. O., Ed.; Academic Press: 1983; Vol. 2, p 346.

(2) (a) Coviello, T.; Kajiwara, K.; Burchard, W.; Dentini, M.; Crescenzi, V. *Macromolecules* **1986**, *19*, 2826. (b) Coviello, K.; Burchard, W.; Dentini, M.; Crescenzi, V. *Macromolecules* **1986**, *20*, 1102. (c) Dentini, M.; Burchard, W.; Crescenzi, V. *Macromolecules* **1988**, *21*, 3312. (d) Coviello, T.; Burchard, W.; Dentini, M.; Crescenzi, V.; Morris, V. J. *J. Polym. Sci., Part B* **1995**, *33*, 1833. (e) Coviello, T.; Burchard, W.; Geissler E.; Maier, D. *Macromolecules* **1997**, *30*, 2008.

(3) (a) Koepsell H. J.; Tsuchiya, H. M. *J. Bacteriol* **1952**, *63*, 293. (b) Jeanes, A.; Wilham, C. A.; Mier, J. C. *J. Biol. Chem*. **1948**, *176*, 603.

(4) Sandford, P. A.; Baird, J. Industrial Utilization of Polysaccharides. In *The Polysaccharides*; Aspinall, G. O., Ed.; Academic Press: 1983; Vol. 2, p 474.

(5) See ref 1, p 346.

(6) Flory, P. J. *Principles of Polymer Chemistry*; Cornell University Press: Ithaca, N. Y., 1953.
(7) Senti, F. Z.; Hellmann, N. N.; Ludwig, N. H.; Babcock, G. E.; Tobin, R.; Glass, C. A.; Lamberts, B. L. *J. Polym. Sci.* **1955**, *17*, 527.
(8) Nordmeier, E. *J. Phys. Chem.* **1993**, *21*, 5770.
(9) (a) Galinsky, G.; Burchard, W. *Macromolecules* **1996**, *29*, 1498. (b) Aberle, T.; Burchard, W. *Starch* **1997**, *49*, 215. (c) Ioan, C. E.; Aberle, T.; Burchard, W. *Macromolecules* **1999**, *32*, 8655. (d) Ioan, C. E.; Aberle, T.; Burchard, W. *Macromolecules*, submitted for publication.
(10) (a) Roessner, D.; Kulicke, W. M. *J. Chromatogr.* **1994**, *687*, 249. (b) Thielking, H.; Kulicke, W. M. *J. Microcolumn Sep.* **1998**, *10*, 51.
(11) Hanselmann, R.; Burchard, W.; Lemmes, R.; Schwengers, D. *Macromol. Chem. Phys.* **1995**, *196*, 2259.
(12) Galinsky, G.; Burchard, W. *Macromolecules* **1995**, *28*, 2363.
(13) Nelson, N. *J. Biol. Chem.* **1944**, *153*, 375.
(14) *Light Scattering from Polymer Solutions*; Huglin, M. B., Ed.; Academic Press: London, New York, 1972.
(15) Bantle, S.; Schmidt, M.; Burchard, W. *Macromolecules* **1982**, *15*, 1604.
(16) (a) Burchard, W. *Macromolecules* **1977**, *10*, 919. (b) Burchard, W. *Adv. Polym. Sci.* **1999**, *143*, 113.
(17) Burchard, W. *Macromolecules* **1972**, *5*, 604.
(18) Weissmüller, M.; Burchard, W. *Polym. Int.* **1997**, *44*, 380.
(19) Yamakawa, H. *Modern Theory of Polymer Solutions*; Harper & Row: New York, 1971.
(20) Hanselmann, R.; Burchard, W.; Ehrat, M.; Widmer, H. M. *Macromolecules* **1996**, *29*, 3277.
(21) Stauffer, D. *Introduction to Percolation Theory*; Taylor & Francis, London, and Philadelphia, PA, 1985.
(22) Freed, K. F. *Renormalization Group Theory of Macromolecules*; Wiley & Sons: New York, 1987.
(23) Kirkwood, J. G.; Riseman, J. *J. Chem. Phys.* **1948**, *16*, 565.
(24) (a) Freire, J. J.; Pla, J.; Rey, A.; Prats, R. *Macromolecules* **1986**, *19*, 452. (b) Freire, J. J.; Rey, A.; Garcia de la Torre, J. *Macromolecules* **1986**, *19*, 457. (c) Rey, A.; Freire, J. J.; Garcia de la Torre, J. *Macromolecules* **1987**, *20*, 347.
(25) Galinsky, G.; Burchard, W. *Macromolecules* **1997**, *30*, 4445.
(26) Burchard, W. *Adv. Polym. Sci.* **1983**, *48*, 1.
(27) Bauer, J.; Burchard, W. *Macromolecules* **1993**, *26*, 3103.
(28) Marriman, H. J.; Hermans, J. J. *J. Phys. Chem.* **1961**, *65*, 385.
(29) Schossler, F.; Benoit, H.; Grubisic-Gallot, Z.; Strazielle, C.; Leibler, L. *Macromoelcules* **1989**, *22*, 400.

MA000282N